Title
An optical coherence tomography (OCT)-based air jet indentation system for measuring the mechanical properties of soft tissues.

Journal
Measurement science & technology, 20(1)

ISSN
0957-0233

Authors
Huang, Yan-Ping
Zheng, Yong-Ping
Wang, Shu-Zhe
et al.

Publication Date
2009

DOI
10.1088/0957-0233/20/1/015805

Published in final edited form as:
Meas Sci Technol. 2009 January ; 20(1): 1–11. doi:10.1088/0957-0233/20/1/015805.

An optical coherence tomography (OCT)-based air jet indentation system for measuring the mechanical properties of soft tissues

Yan-Ping Huang[1], **Yong-Ping Zheng**[1,2], **Shu-Zhe Wang**[1], **Zhong-Ping Chen**[3], **Qing-Hua Huang**[1], and **Yong-Hong He**[4]

Yong-Ping Zheng: ypzheng@ieee.org; Qing-Hua Huang: hti.huang@polyu.edu.hk

[1]Department of Health Technology and Informatics, Hong Kong Polytechnic University, Hong Kong, People's Republic of China

[2]Research Institute of Innovative Products and Technologies, Hong Kong Polytechnic University, Hong Kong, People's Republic of China

[3]Beckman Laser Institute, University of California Irvine, Irvine, CA, USA

[4]Graduate School at Shenzhen, Tsinghua University, Shenzhen, People's Republic of China

Abstract

A novel noncontact indentation system with the combination of an air jet and optical coherence tomography (OCT) was presented in this paper for the quantitative measurement of the mechanical properties of soft tissues. The key idea of this method is to use a pressure-controlled air jet as an indenter to compress the soft tissue in a noncontact way and utilize the OCT signals to extract the deformation induced. This indentation system provides measurement and mapping of tissue elasticity for small specimens with high scanning speed. Experiments were performed on 27 silicone tissue-mimicking phantoms with different Young's moduli, which were also measured by uniaxial compression tests. The regression coefficient of the indentation force to the indentation depth (N mm^{-1}) was used as an indicator of the stiffness of tissue under air jet indentation. Results showed that the stiffness coefficients measured by the current system correlated well with the corresponding Young's moduli obtained by conventional mechanical testing ($r = 0.89$, $p < 0.001$). Preliminary *in vivo* tests also showed that the change of soft tissue stiffness with and without the contraction of the underlying muscles in the hand could be differentiated by the current measurement. This system may have broad applications in tissue assessment and characterization where alterations of mechanical properties are involved, in particular with the potential of noncontact micro-indentation for tissues.

Keywords

indentation; ultrasound indentation; soft tissue; elasticity; air jet; optical coherence tomography

1. Introduction

In many tissue pathologies such as fibrosis, edema and cancers in breast, liver and prostate, change of mechanical properties [1–4] is a common phenomenon observed by clinicians or patients themselves using hand palpation. However, the hand palpation method is qualitative, at most semi-quantitative (such as the scoring system from the palpation impression), thus limiting its use in quantitative and objective studies. In the last two decades, in order to find optimal modalities for disease diagnosis and tissue assessment, more and more researchers have put efforts in developing quantitative and objective approaches in the field of elasticity measurement and imaging based on ultrasound [5–15], MRI [16] or optical [17–22]

measurements with the help of some kind of mechanical disturbances caused to the tissues including compression, indentation, suction, vibration or acoustic radiation.

Indentation is currently one of the most frequently used techniques to measure the biomechanical properties of soft tissues [23,24]. Indentation, due to a small contact area with the tested objective, has the advantages of no necessity to excise the particular tissue, which is almost impossible for a standard uniaxial compression test, thus allowing its especial use for *in vivo* applications. A traditional indentation system used a rigid indenter to compress the tissue in order to characterize the mechanical properties of soft tissue using the relationship between force and deformation. However, usually no thickness information could be obtained directly from the indentation test. Tissue thickness is an important parameter for the diagnosis of some tissue pathologies such as cartilage degeneration [25], and is also an important factor for the calculation of tissue stiffness because this is included in the boundary condition of the theoretical analysis of the indentation test [23]. The thickness was usually measured by extra post-test methods such as the needle probe penetration [26]. To address this issue, Zheng and Mak [7] developed a portable ultrasound indentation system, which used the ultrasound transducer itself as an indenter. The system is capable of measuring both the initial thickness and stiffness. Due to its easy operation and a relatively compact profile fit for clinical operations, this ultrasound indentation system has been successfully applied in the assessment of a variety of tissues *in vivo*, including muscular tissues [27], residual limb tissues [28], diabetic foot plantar tissues [29], neck tissue fibrosis induced by radiotherapy [30,31], hypertrophic scar tissues [32,33] and carpal tunnel ligament [34]. Similar ultrasound indentation has also been used for the assessment of articular cartilage [35,36].

Typical ultrasound indentation uses an ultrasound transducer with the central frequency of 2–10 MHz for which the resolution is quite limited for small specimens such as the skin and articular cartilage. For transducers with a higher frequency, the end is normally concave for better energy focus and larger penetration depth. In this case, the transducer tip cannot be used directly as an indenter. Introduction of a bolster at the transducer tip for a planar indentation surface may possibly induce a poor coupling of the ultrasound signal and significantly attenuate the ultrasound signal, which severely affects the ultrasound measurement [36]. In addition, a rigid indenter is limited in achieving a fast scanning speed because of the requirement of pointwise measurement. To address these issues, a water jet indentation system was developed [37,38]. In this system, the water jet serves as both the indenter and the coupling medium, thus significantly improving the speed in a C-scan test, i.e. the imaging plane is perpendicular to the ultrasound beam [38]. Phantom tests showed that this system was capable of measuring the soft tissue elasticity quantitatively and reliably and also providing a fast C-scan mapping of the tissue elasticity. It was further applied for the study of cartilage degeneration in a bovine patella model [39] and bone–tendon junction healing in a rabbit model [40] *in vitro*. The noncontact fluid indentation method also has the advantage of lowering the potential or risk of causing damage to the tested soft tissue, especially in tissues such as in scars or wounds where the contact indenter may cause inflammatory effects. Almost at the same time, another group reported a similar system using a water jet for the assessment of articular cartilage [19]. They used an optical technique to detect the deformation applied by the water jet on the cartilage surface. Briefly, an optical beam with a constant intensity was illuminated onto the cartilage surface, and reflecting light was collected and its intensity was related to the local surface curvature, which was caused by the compression of the water jet.

One inconvenience in using the water jet indentation is that the water will spill all over during the test. If it is used for tissues located inside a body, the water or saline needs to be removed by another instrument. Another important factor for the widespread applications of prototype biomedical instrumentations to clinical situations is the potential of device miniaturization [41]. Even though miniaturization of ultrasound transducers is possible, such as those used for

an intra-vascular ultrasound imaging system, it is very expensive and the resolution is inherently limited. The water jet optical measurement system [19] used the intensity of the reflecting light to measure tissue deformation, but it is not accurate, particularly when the deformation is large or the tissue surface has different colors and textures.

In various optical methods, optical coherence tomography (OCT) is a recent and fast developing technique that has acquired more and more widespread use in biomedical research [42]. The principle of OCT itself is analogous to that of pulse-echo ultrasound imaging. It collects backscattered signals from the optically scattering tissues for the purpose of cross-sectional imaging. The difference with respect to ultrasound is that OCT uses the optical interferometric rather than the absolute time of flight technique to resolve the spatial information. OCT uses an optical interferometric method with a small coherence length of the light source and can achieve a high resolution. Axial and lateral resolutions in a range of several microns can be achieved, thus making the optical biopsy a unique and attractive characteristic of this technique [43–45]. Similar to the ultrasound signals, the OCT can measure the thickness of tissue layers where normally at the interfaces the refractive index is abruptly changed. For example, one of the most important applications of OCT is pachymetry, i.e., to measure the corneal thickness *in vivo* for the use of diagnosis or surgery guide [46,47]. OCT-based elasticity imaging for tissues has also been widely investigated using contact compression [18,20,21]. In comparison with ultrasound elastography, the OCT-based technique can provide higher resolutions. However, these elasticity imaging techniques can normally provide contrast of local strains but not an absolute value of tissue elasticity.

The integration of an OCT probe with the air jet indentation was realized in the current study to develop a novel system to measure the mechanical properties of soft tissues. First, the construction of the system is described in the next section, then experimental and data analysis methods on phantoms and *in vivo* hand soft tissues, and the corresponding results are presented to demonstrate the utility of the current system, and finally further issues related to the limitations, further improvement and applications of the current system in biomedical engineering are discussed before the study is concluded.

2. Methods

2.1. System setup

The schematic of the OCT-based air jet indentation system including the core part and the data collection part is shown in figures 1 and 2, respectively. The fiber-based OCT probe was modified to allow the installation of an air jet bubbler. The OCT system (developed by Lab of Optical Imaging and Sensing, Graduate School at Shenzhen, Tsinghua University, China) has a super luminescent diode (SLD) light source (DenseLight, DL-CS3055 A, Singapore) with a central wavelength of 1310 nm, a nominal −3 dB spectral bandwidth of 50 nm and a nominal output power of 5 mW. The axial resolution is 18 μm and the imaging depth is approximately 2–3 mm in turbid high scattering tissues. The OCT probe was fixed in this study and the laser beam focuses vertically at around 5 mm under the lower surface of the bubbler. For convenience of detection, a visible red light beam was used with the invisible infrared beam to guide the detection point. A pipeline with maximally constant air pressure was connected to the system to provide the air jet for the indentation. To make the air jet more uniform, a tube with an orifice diameter of 2 mm and a length of 5 mm was installed at the tip of the bubbler to guide the air jet before it was pushed into free space. A calibrated pressure sensor (PMP 1400, GE Druck, Leicester, England) with a measurement range of 1 bar (10^5 Pa) was installed before the bubbler to measure the pressure in the air pipe. A mechanical valve was installed before the pressure sensor to adjust the pressure of the air jet continuously. A transparent plate was installed at the top of the bubbler to seal the pressurized air from the OCT components but let the laser beam pass through.

A PC was used to control the operation of the system. A data acquisition card (DAQ, PCI-6251, National Instruments, Austin, TX, USA) was used through intercommunication to both control the main unit of OCT and collect the optical signals. Another DAQ card (PCI-6024E, National Instruments, Austin, TX, USA) was used to collect the signal from the pressure sensor. A custom-written program was developed in Microsoft VC++ for the signal synchronization and data collection (figure 3). During the indentation process, the signals from the OCT and the pressure sensor were synchronized, sampled, displayed in real time and saved for off-line processing by the program. In this study, the OCT scanning was continuously performed at a single location to track the surface displacement, which was assumed to be equivalent to the deformation of the tested specimen. The digitized A-scan signalwas acquired at a rate of approximately 3.1 Hz and the pressure signal was also sampled at this rate in synchronization with the A-scan signal. Each A-scan signal contained 7500 points of effective digital data for analysis. By using the two surfaces of a glass slide with a standard thickness for distance calibration, we obtained an equivalence of 0.43 μm per point for each A-line of the signal in air after calibration considering the difference of the refractive indices in glass and air. The displacement of the surface was extracted by applying a cross-correlation algorithm to the A-line signals, which was used to seek the most similar part to a pre-selected region of interest (ROI) in the A-scan signals recorded during the indentation process. The air–specimen interface was used as the pre-selected ROI in this study. In order to reduce the effect of the signal phase change during indentation and assure better tracking, the amplitude signal obtained by applying a Hilbert transform to the original optical signal was employed for the tracking. The same software using a different control panel was used to conduct the algorithms of cross-correlation for the extraction of the deformation (figure 3).

2.2. Phantoms and in vivo tests

We tested the system on 27 uniform tissue-mimicking silicone phantoms with different stiffness. They were made of three kinds of silicone materials with low viscosity: Rhodia RTV 573 (Rhodia Inc., CN7500, Cranbury, NJ, USA), Wacker M4648 and M4640 (Wacker Chemicals Hong Kong Ltd, Hong Kong, China). For each type of silicone, there were two parts A and B before mixing to make the phantom. Different proportions of A and B were mixed to make phantoms with different stiffness. Here we chose three different silicone materials to make phantoms covering a wide range of stiffness because phantom stiffness was dependent not only on the mixing ratio of the two parts but also on the silicone type. Three categories of phantom dimensions with a surface area of 10×10 mm^2 and thicknesses of 5, 10 and 15 mm were fabricated [37]. All the experiments were conducted on the 10×10 mm^2 surface but with different phantom initial thicknesses (5, 10 or 15 mm). During the air jet indentation, the phantom was fixed at the edges by four screws and the air jet was exerted at the center of the surface. For each phantom, the axial distance of the phantom surface to the bubbler bottom was adjusted to be approximately 5 mm based on the optical signal detected from the surface. If the specimen were too close to the bubbler, it would be attracted toward the bubbler by a force induced by the high velocity of the scattered air jet and the low pressure incurred around. Before each indentation, the phantom was compressed and relaxed several times to obtain a rigid fixation on the platform. Then the air jet indentation was exerted at a pressure changing rate of approximately 10 kPa s^{-1} and between 0 and 100 kPa, which corresponded to a maximum displacement of about 0.37 mm for the softest phantom. The maximum indentation depth was less than 5% for the phantom test. A typical test, including 1 to 2 cycles of indentation, was finished in approximately 30 s. For the purpose of comparison, indentation tests with a rigid steel indenter (called standard indentation) and standard compression tests were also performed using a standard mechanical testing machine (Instron 5569, Norwood, MA,USA). For these two mechanical tests, the maximum indentation or compression depth was about 10% of the initial thickness (only the data within 3% deformation were used for

parameter calculation) and the indentation speed was controlled to be 4 mm min^{-1}, which was similar to that of the air jet indentation.

In order to demonstrate the biomechanical applications of the system, a preliminary test was performed on soft tissues of the hand *in vivo* to differentiate the contraction state of the underlying muscle layer involved. Ten subjects (seven males, three females) without any lesions in the hand and with a mean age of 27.8 ± 2.9 years (minimum: 23; maximum 32) were recruited in this test. A test site near the basal joint of the dorsal hand including the muscles of the first interosseous was selected for the experiment (figure 4). The subjects were asked to be seated in a natural posture with their hand placed on the platform. Two states of the muscle, i.e. relaxation and contraction, were produced by natural extension and forced adduction of the thumb (figure 4). A deformation of approximately 1.5 mm was applied on the tissues using the air jet. The corresponding indentation deformation and forces were then collected and used for the calculation of the stiffness parameter.

2.3. Data analysis method

In the current study, the air jet indentation was assumed to be similar to the indentation with a rigid contact by hypothesizing that the air pressure measured in the pipe was linearly proportional to the force induced on the specimen. The proportionality of the fluid pressure and the indentation force was earlier validated for the water jet case [37]. For the phantom tests, a stiffness coefficient k_{aj} (N mm^{-1}) regarding the regression ratio of the air jet indentation force (N) and deformation (mm) of the tested specimen was used to represent the stiffness of the phantom. This parameter was used here because with the assumption of linear elasticity, a constant Poisson's ratio and a small aspect ratio (indenter radius/initial thickness a/h, in this study always less than 0.2), the indentation formula was [23]

$$E=(1-\upsilon^2)/(2a\kappa(\nu,a/h))\cdot F/d \tag{1}$$

where E is Young's modulus of the tissue, a is the radius of the indenter, h is the initial thickness of the tissue, ν is Poisson's ratio of the tissue, κ is a scaling factor related to ν and a/h, F is the indentation force and d is the indentation depth. For the elastic material, equation (1) is simplified to

$$E=(1-\nu^2)/(2a)\cdot F/d, \tag{2}$$

with κ approaching to 1 in equation (1) [23,29,48]. The indentation force was computed by multiplying the measured air pressure with the area of the bubbler orifice ($\phi = 2a = 2$ mm). The corresponding stiffness coefficient obtained by the standard indentation was indicated by k_{std}. For the standard compression test, Young's modulus (E) of phantom could be obtained after computing the corresponding stress and strain. We assumed homogeneity of the compressive properties of the phantom, so one value of Young's modulus would represent all at each specific point. The deformation ratio (deformation/initial thickness) or strain was constrained to be within 3% in all the calculations in order to obtain a coefficient within the linear elasticity region of compression of the phantoms [49]. Due to low viscosity of the silicone phantoms, data of both the loading and unloading processes were utilized for the calculation of the stiffness coefficient. The Pearson correlation coefficient was used to indicate the relationship among the measured parameters from the air jet indentation, the standard indentation and compression test.

For the *in vivo* test, a corresponding stiffness coefficient k (N mm^{-1}) regarding the force/deformation ratio was calculated from the test, and the average value of three repeated tests

was used for each muscle contraction state. It should also be noted that the mechanical properties measured from the hand soft tissue were characteristic of the whole tissue layer which might include layers of skin, fat and muscles, but not that of a separate single layer. When the whole tissue layer undergoes some pathological or physiological changes such as muscle contraction in the current study, the whole tissue will behave differently. Therefore, the measurement of overall tissue properties is also meaningful for the detection of the tissue state under these conditions. A paired *t*-test was used to compare the change of the stiffness coefficient *k* for the soft tissues with and without muscle contraction. All the statistical analyses were performed in SPSS 14.0 (SPSS, Chicago, IL, USA). In all the statistical tests, $p < 0.05$ was used to indicate a significant correlation or a significant difference of the mean between two measures.

3. Results

The results of a representative indentation test on the phantom are shown in figure 5. Using the cross-correlation algorithm, the displacement could be successfully extracted during the indentation in the phantom tests. Some noise with the extracted deformation was found during the processing, the reason for which is discussed in detail in the next section. A high correlation coefficient, normally larger than 0.95, was observed for the indentation force and deformation. A reliability test of ten times repeated experiments on one phantom showed that k_{aj} was 1.108 ± 0.035 N mm^{-1} (3.2% for the coefficient of variation), which in turn showed that the test was highly reliable. Correlation tests among k_{aj}, k_{std} and E are shown in figure 6. A high correlation of $r = 0.88$ ($p < 0.001$) was found for k_{aj} and k_{std}, which showed that the results of the two tests were highly comparable. A larger value of k_{aj} was consistently observed from the air jet indentation system than k_{std}, which might be attributed to the fact that a larger pressure was measured inside the air pipe than at the surface of the specimen where the air jet induced the deformation. The compression test showed that the stiffness of the phantoms was 558 ± 124 kPa with a range of 328–818 kPa. A comparison between k_{aj} and E also showed a high correlation ($r = 0.89$, $p < 0.001$), which indicated that the current system could be used as a new approach to measure the mechanical properties of soft tissues.

The *in vivo* test showed that the stiffness coefficient was 0.059 ± 0.031 N mm^{-1} and 0.150 ± 0.059 N mm^{-1} with the muscle in the relaxation and contraction states, respectively. A paired *t*-test showed that the soft tissue was significantly stiffer in the state of muscle contraction ($p < 0.001$). Therefore, the current system was capable of differentiating the state of the muscle contraction.

4. Discussion

An air jet indentation system utilizing the optical signals from the OCT system was developed and tested to demonstrate its capability in measuring the mechanical properties of soft tissues. Preliminary results on silicone phantoms and *in vivo* soft tissues of the hand showed that it was feasible to use the air jet indentation system to quantitatively measure the stiffness and further to detect the change of stiffness that might be involved in various tissue pathologies. The air jet was thought to be very convenient for use, because no extra mechanism was needed to collect the spilt medium, as in the water jet case. The incorporation of the OCT signal enabled the detection of deformation (displacement) as small as less than 1 μm, and provided the potential for miniaturization for use in applications such as endoscopy. Compared to the rigid contact indentation method, this novel air jet indentation system also provided a potential for testing in fine tissues and a fast scanning to map the deformation distribution in soft tissues.

In the current study, OCT signals were introduced to extract the deformation of the indented specimen. The deformation was obtained by assuming that the platform underlying the

specimen was fixed and then it was equivalent to track the surface movement. In real situations, the deformation as well as the thickness of the tissue can be measured directly from the OCT signal, provided that the whole tissue layer can be penetrated by the optical beam. This is also the advantage of using OCT for the air-jet measurement system in comparison with other optical methods for surface displacement measurement. In the current study, the measured stiffness coefficient represented the mechanical properties of the whole tissue layer. During data processing, it was found that the optical signals were quite sensitive to the movement of the surface of the specimen, even in the phantom test where the phantoms were firmly fixed. This might be caused by the surface roughness of the skin and the orientation change of the optical beam with non-vertical incidence during indentation. This sensitivity had brought some noise to the deformation in tracking. When necessary, the moving average was used in the current study to reduce the effect of noise. The movement sensitivity was one of the big differences noted by us between the OCT and ultrasound signals. We had not encountered such a problem previously in processing the ultrasound signal. This might be due to the uncertain change of the phases in the OCT signals with respect to the surface signal. This sensitivity might induce some tracking challenges in experiments, particularly tests on tissues *in vivo*, where the tissue self-motion during indentation is inevitable such as that caused by the respiration and heartbeat. Therefore, in the current design of the soft tissue test *in vivo*, a roughly constant indentation depth was produced by the air jet and then we measured the corresponding force in order to calculate the stiffness coefficient. Another issue for using the cross-correlation algorithm was the decorrelation caused by a large displacement. However, we thought the effect of decorrelation might not be so significant in the current study due to two main reasons: one was that the envelop signal was obtained to exclude or reduce the effect of the phase change in tracking; the other was that we only detected the abrupt change of the surface signal, which was relatively easier to track by choosing the ascending part of the signal at the surface. The sensitivity of the signal shape and signal to noise ratio to the movement tracking of the specimen surface and approaches for lowering this sensitivity for a more reliable tracking need to be further investigated.

The axial resolution of the OCT system used in this study was 18 μm, which was the limit for the system to differentiate signals generated by two neighboring interfaces. Since in the current study we were interested in the movement of a distinguished interface, i.e. phantom surface or skin surface, we were able to achieve a much higher displacement resolution beyond the axial resolution, given that the decorrelation of the signal was small. The displacement resolution for the distinguished surface was mainly determined by the number of data points for a certain period of the OCT signal, which represented a certain distance in the medium. In this study, we collected 7500 data points for a distance of approximately 3.22 mm (this value depends on the refractive index of the medium). Therefore, the displacement resolution of the interface movement was approximately 0.43 μm. Such a displacement resolution for interface tracking can be achieved even when the OCT signals generated by two neighboring interfaces overlapped, i.e. the distance between the two interfaces is smaller than the axial resolution of the measurement system, given that the two interfaces have no relative motion during the movement. However, the displacement resolution discussed above cannot be applied to the movements of interfaces with the distance smaller than the axial resolution and involving relative motions, as this will cause decorrelation of the OCT signals. Under this condition, we are not able to tell which interface contributes to the displacement of the signal and the displacement resolution will be significantly reduced. The above discussion can not only be applied to the movement of the surface interfaces but also to those inside the media. Apparently, the displacement resolution of 0.43 μm for the interface movement cannot be applied to the movement of scatters inside the medium, as the distances between scatters are very small and a smaller relative motion among them will cause large decorrelation to the signal. That is why the displacement resolution for ultrasound elastography [5], which aims to map tissue displacement or strain but not to measure the displacement of a certain interface, is normally

limited by the axial resolution of the imaging system. In addition to signal decorrelation, cross-correlation tracking for signals can also be affected by the signal to noise ratio and the sampling rate of the signals. To measure tissue motion more accurately, it is worthwhile to systematically investigate the displacement resolution of the proposed OCT air jet system for the tissue interface and scatters inside the tissue in future studies.

A single point of displacement was measured in the current study using the A-line OCT signal to obtain the deformation of the whole specimen layer. In further studies, cross-sectional scanning, as used in B-mode ultrasound imaging, can be used to further study the problem such as the deformation profile under the air jet as long as the lateral scanning can cover the size of the bubbler orifice. The frame rate of the OCT A-line used in this study was relatively low. Though it did not affect the measurement for the phantoms and the carefully selected region of the hand, it should be significantly improved when cross-sectional scanning is required. Utilizing the cross-sectional imaging, elastography, which has been studied extensively in ultrasound and MR imaging fields [5,16], can also be performed, provided the air jet induces the required deformation of the specimen [18]. One of the advantages of OCT compared to ultrasound is that OCT is easier for minimization due to the fast development of optical technologies and devices. OCT probes for endoscopic use in human mucosa have already been reported in the literature [50,51]. Therefore, another aspect for further development is the minimization of the air jet indentation system for portable or endoscopic uses [50–52]. In such cases, the probe can be portable for flexible use in various body sites or small enough to be inserted in endoscopy for internal tissue detection.

A hypothesis of the current study was that the air jet indentation was comparable to the standard indentation with a rigid indenter and then the stiffness of specimen was simplified in an index coefficient of the force/deformation ratio. The high correlation of the stiffness coefficients between the air jet indentation and standard indentation showed that these two tests really were similar. The high correlation between the stiffness coefficient and Young's modulus showed in a further step that the stiffness coefficient could be used as a quantitative measure of the specimen elasticity. Thus, the developed OCT-based air jet indentation system can be further applied to a host of body tissues for clinical diagnoses, such as skin cancer, burn status, corneal condition, blood vessel stiffening and articular cartilage degeneration, where the change of tissue elasticity is obviously involved from clinical observations.

However, intrinsic mechanical properties such as Young's modulus are more preferable for widespread applications, because this will further enable the inter-lab or inter-hospital comparisons of respective studies. Therefore, further investigations are needed to extract the intrinsic mechanical properties from the air jet indentation test. This is thought to be complicated due to two main reasons: complicated mechanical behavior of the soft tissues under rigid indentation, and the complicated interactions between the air jet and the soft tissues in air jet indentation. The first issue was addressed previously in a lot of studies [23,48,53–55]. In linear elasticity theory, the factors that affect the extraction of the elastic modulus include Poisson's ratio, indenter shape, force/indentation ratio and the initial thickness. When the theory is applied to real tissues *in vivo*, careful protocols should be designed to account for the extra effects from viscoelasticity, nonlinearity, non-homogeneity and anisotropy of the tissue properties. In this study, homogeneous and isotropic silicone phantoms were fabricated so as to simplify the mechanical behavior of the specimen. The stiffness coefficient or Young's modulus was obtained with the constraint of 3% of the deformation/thickness ratio or strain, which was thought to be a linear elasticity region for most soft tissues [49]. The viscosity was neglected in the study because it was not so obviously observed for the silicone phantoms fabricated in this study.

On the other hand, the interactions between the air jet and soft tissues are much less studied because the air jet indentation for the measurement of tissue elasticity was a novel approach in the biomedical engineering field. Waterjetting, similar to the air jet, is a technique which has found widespread applications in a variety of industries [56]. However, the previous analysis on waterjetting could not be directly applied to our studies because most of the industrial applications focus on material cutting and cleaning, where the water pressure is much higher than that used in the current study. The difference between the rigid indention and air jet indentation is that the tissue under the rigid indenter is uniformly compressed with a planar surface in the former case while this may not be true for the air jet. It is expected that the deformation profile as well as the pressure distribution in the interaction surface keeps changing with the change of the air jet pressure. Finite element analysis, as used in previous indentation studies [57–60], may be incorporated in further studies for the analysis of the air jet indentation to investigate the interactions between the air jet and tissues and the effects of the variations including Poisson's ratio, the air jet radius, the distance between the bubbler tip and the tissue surface, and the tissue thickness.

5. Conclusion

A novel OCT-based air jet indentation system was developed in the current study. OCT can be used to detect tissue deformation as small as submicrons in a noncontact way. The high correlation of the stiffness measured by the current system with that obtained by the conventional and standard methods indicated that a mechanical test with the OCT-based air jet indentation was feasible. The capacity of the system to detect biomechanical changes in soft tissues was demonstrated by a phantom study and a preliminary *in vivo* test. Further improvements are required to include lateral scanning functions so as to map the tissue elasticity and to enhance the stability of the OCT signal from the skin surface for *in vivo* applications where motion artifacts cannot be avoided. The combination of the proposed air jet technique and the OCT elastography methods recently reported in the literature [18,20,21,61,62] may be able to provide noncontact OCT elasticity imaging for tissues. Testing on more tissues to demonstrate the potential of this system for widespread applications in biomedical engineering is under planning.

Acknowledgments

We would like to thank the contributions from Mr Chi-Fai Tin in the workshop of HTI Department, Hong Kong Polytechnic University, for the setup of the system. This work was partially supported by Hong Kong Research Grants Council (PolyU5318/05E) and the Hong Kong Polytechnic University (J-BB69).

References

1. Mridha M, Odman S. Noninvasive method for the assessment of subcutaneous edema. Med. Biol. Eng. Comput 1986;24:393–398. [PubMed: 3796070]
2. Garra BS, Cespedes EI, Ophir J, Spratt SR, Zuurbier RA, Magnant CM, Pennanen MF. Elastography of breast lesions: initial clinical results. Radiology 1997;202:79–86. [PubMed: 8988195]
3. McKnight AL, Kugel JL, Rossman PJ, Manduca A, Hartmann LC, Ehman RL. MR elastography of breast cancer: preliminary results. Am. J. Roentgenol 2002;178:1411–1417. [PubMed: 12034608]
4. Davis AM, Dische S, Gerber L, Saunders M, Leung SF, O'Sullivan B. Measuring postirradiation subcutaneous soft-tissue fibrosis: state-of-the-art and future directions. Semin. Radiat. Oncol 2003;13:203–213. [PubMed: 12903010]
5. Ophir J, Cespedes I, Ponnekanti H, Yazdi Y, Li X. Elastography—a quantitative method for imaging the elasticity of biological tissues. Ultrason. Imaging 1991;13:111–134. [PubMed: 1858217]
6. Parker KJ, Gao L, Lerner RM, Levinson SF. Techniques for elastic imaging: a review. IEEE Eng. Med. Biol 1996;15:52–59.

7. Zheng YP, Mak AFT. An ultrasound indentation system for biomechanical properties assessment of soft tissues *in-vivo*. IEEE Trans. Biomed. Eng 1996;43:912–918. [PubMed: 9214806]
8. Fatemi M, Greenleaf FJ. Ultrasound-stimulated vibro-acoustic spectrography. Science 1998;280:82–85. [PubMed: 9525861]
9. Sarvazyan AP, Rudenko OV, Swanson SD, Fowlkes JB, Emelianov SY. Shear wave elasticity imaging—a new ultrasonic technology of medical diagnostics. Ultrasound Med. Biol 1998;24:1419–1435. [PubMed: 10385964]
10. Diridollou S, Patat F, Gens F, Vaillant L, Black D, Lagarde JM, Gall Y, Berson M. *In vivo* model of the mechanical properties of the human skin under suction. Skin Res. Technol 2000;6:214–221. [PubMed: 11428960]
11. Nightingale KR, Palmeri ML, Nightingale RW, Trahey GE. On the feasibility of remote palpation using acoustic radiation force. J. Acoust. Soc. Am 2001;110:625–634. [PubMed: 11508987]
12. Sandrin L, Tanter M, Gennisson JL, Catheline S, Fink M. Shear elasticity probe for soft tissues with 1-D transient elastography. IEEE Trans. Ultrason. Ferroelectr. Freq. Control 2002;49:436–446. [PubMed: 11989699]
13. Zheng YP, Mak AFT, Lau KP, Qin L. An ultrasonic measurement for *in vitro* depth-dependent equilibrium strains of articular cartilage in compression. Phys. Med. Biol 2002;47:3165–3180. [PubMed: 12361216]
14. Konofagou EE, Hynynen K. Localized harmonic motion imaging: theory, simulations and experiments. Ultrasound Med. Biol 2003;29:1405–1413. [PubMed: 14597337]
15. Zheng YP, Bridal SL, Shi J, Saied A, Lu MH, Jaffre B, Mak AFT, Laugier P. High resolution ultrasound elastomicroscopy imaging of soft tissues: system development and feasibility. Phys. Med. Biol 2004;49:3925–3938. [PubMed: 15470914]
16. Muthupillai R, Lomas DJ, Rossman PJ, Greenleaf JF, Manduca A, Ehman RL. Magnetic resonance elastography by direction visualization of propagating acoustic strain waves. Science 1995;269:1854–1857. [PubMed: 7569924]
17. Asserin J, Agache P, Humbert P. Checking the mechanical performances of a skin suction meter—the cutometer. J. Invest. Dermatol 1995;104:165.
18. Schmitt JM. OCT elastography: imaging microscopic deformation and strain of tissue. Opt. Express 1998;3:199–211. [PubMed: 19384362]
19. Duda GN, Kleemann RU, Bluecher U, Weiler A. A new device to detect early cartilage degeneration. Am. J. Sports. Med 2004;32:693–698. [PubMed: 15090387]
20. Khalil AS, Chan RC, Chau AH, Bouma BE, Mofrad MRK. Tissue elasticity estimation with optical coherence elastography: toward mechanical characterization of *in vivo* soft tissue. Ann. Biomed. Eng 2005;33:1631–1639. [PubMed: 16341928]
21. Kirkpatrick SJ, Wang RK, Duncan DD, Kulesz-Martin M, Lee K. Imaging the mechanical stiffness of skin lesions by *in vivo* acousto-optical elastography. Opt. Express 2006;14:9770–9779. [PubMed: 19529368]
22. Mazza E, Nava A, Halmloser D, Jochum W, Bajka M. The mechanical response of human liver and its relation to histology: an *in vivo* study. Med. Image Anal 2007;11:663–672. [PubMed: 17719834]
23. Hayes WC, Herrmann G, Mockros LF, Keer LM. A mathematical analysis for indentation tests of articular cartilage. J. Biomech 1972;5:541–551. [PubMed: 4667277]
24. Lyyra T, Jurvelin J, Pitkanen P, Vaatainen U, Kiviranta I. Indentation instrument for the measurement of cartilage stiffness under arthroscopic control. Med. Eng. Phys 1995;17:395–399. [PubMed: 7670702]
25. Stahl R, Blumenkrantz G, Carballido-Gamio J, Zhao S, Munoz T, Le Graverand-Gastineau MPH, Li X, Majumdar S, Link TM. MRI-derived T2 relaxation times and cartilage morphometry of the tibio-femoral joint in subjects with and without osteoarthritis during a 1-year follow-up. Osteoarthr. Cartilage 2007;15:1225–1234.
26. Appleyard RC, Burkhardt D, Ghosh P, Read R, Cake M, Swain MV, Murrell GAC. Topographical analysis of the structural, biochemical and dynamic biomechanical properties of cartilage in an ovine model of osteoarthritis. Osteoarthr. Cartilage 2003;11:65–77.
27. Zheng YP, Mak AFT. Effective elastic properties for lower limb soft tissues from manual indentation experiment. IEEE Trans. Rehabil. Eng 1999;7:257–267. [PubMed: 10498372]

28. Zheng YP, Mak AFT, Lue BK. Objective assessment of limb tissue elasticity: development of a manual indentation procedure. J. Rehabil. Res. Dev 1999;36:71–85. [PubMed: 10661523]
29. Zheng YP, Choi YKC, Wong K, Chan S, Mak AFT. Biomechanical assessment of plantar foot tissue in diabetic patients using an ultrasound indentation system. Ultrasound Med. Biol 2000;26:451–456. [PubMed: 10773376]
30. Leung SF, Zheng YP, Choi CYK, Mak SSS, Chiu SKW, Zee B, Mak AFT. Quantitative measurement of post-irradiation neck fibrosis based on the Young modulus—description of a new method and clinical results. Cancer 2002;95:656–662. [PubMed: 12209759]
31. Huang YP, Zheng YP, Leung SF. Quasilinear viscoelastic parameters of neck tissues with fibrosis induced by radiotherapy. Clin. Biomech 2005;20:145–154.
32. Lau J, Li WPC, Zheng YP. Application of tissue ultrasound palpation system (TUPS) in objective scar evaluation. Burns 2005;31:445–452. [PubMed: 15896506]
33. Li-Tsang CWP, Lau JCM, Chan CCH. Prevalence of hypertrophic scar formation and its characteristics among the Chinese population. Burns 2005;31:610–616. [PubMed: 15993306]
34. Zheng YP, Li ZM, Choi APC, Lu MH, Chen X, Huang QH. Ultrasound palpation sensor for tissue thickness and elasticity measurement—assessment of transverse carpal ligament. Ultrasonics 2006;44:e313–e317. [PubMed: 16844164]
35. Suh JKF, Youn I, Fu FH. An *in situ* calibration of an ultrasound transducer: a potential application for an ultrasonic indentation test of articular cartilage. J. Biomech 2001;34:1347–1353. [PubMed: 11522315]
36. Laasanen MS, Saarakkala S, Toyras J, Hirvonen J, Rieppo J, Korhonen RK, Jurvelin JS. Ultrasound indentation of bovine knee articular cartilage *in situ*. J. Biomech 2003;36:1259–1267. [PubMed: 12893034]
37. Lu MH, Zheng YP, Huang QH. A novel noncontact ultrasound indentation system for measurement of tissue material properties using water jet compression. Ultrasound Med. Biol 2005;31:817–826. [PubMed: 15936497]
38. Lu MH, Zheng YP, Huang QH. A novel method to obtain modulus image of soft tissues using ultrasound water jet indentation: a phantom study. IEEE Trans. Biomed. Eng 2007;54:114–121. [PubMed: 17260862]
39. Lu MH, Zheng YP, Huang QH, Ling HY, Wang Q, Bridal SL, Qin L, Mak AFT. Noncontact evaluation of articular cartilage degeneration using a novel ultrasound water jet indentation system. Ann. Biomed. Eng. 2008 at press.
40. Lu MH, Zheng YP, Lu HB, Huang QH, Qin L. A noncontact ultrasound method for evaluation of bone-tendon junction healing. Ultrasound Med. Biol. 2008 Under review.
41. Cote GL, Lec RM, Pishko MV. Emerging biomedical sensing technologies and their applications. IEEE Sensors J 2003;3:251–266.
42. Huang D, et al. Optical coherence tomography. Science 1991;254:1178–1181. [PubMed: 1957169]
43. Drexler W. Ultrahigh-resolution optical coherence tomography. J. Biomed. Opt 2004;9:47–74. [PubMed: 14715057]
44. Leitgeb RA, Drexler W, Unterhuber A, Hermann B, Bajraszewski T, Le T, Stingl A, Fercher AF. Ultrahigh resolution Fourier domain optical coherence tomography. Opt. Express 2004;12:2156–2165. [PubMed: 19475051]
45. Chen ZP, Zhao YH, Srivivas SM, Nelson JS, Prakash N, Frostig RD. Optical Doppler tomography. IEEE J. Sel. Top. Quantum Electron 1999;5:1134–1142.
46. Bohnke M, Masters BR, Walti R, Ballif JJ, Chavanne P, Gianotti R, Salathe RP. Precision and reproducibility of measurements of human corneal thickness with rapid optical low-coherence reflectometry (OLCR). J. Biomed. Opt 1999;4:152–156.
47. Tomlins PH, Wang RK. Theory, developments and applications of optical coherence tomography. J. Phys. D: Appl. Phys 2005;38:2519–2535.
48. Waters NE. Indentation of thin rubber sheets by cylindrical indentors. Br. J. Appl. Phys 1965;16:1387–1392.
49. Nitta N, Shiina T. A visualization of nonlinear elasticity property of tissues by ultrasound. Electron. Commun. Japan 2002;85:9–18.

50. Sergeev A, et al. *In vivo* endoscopic OCT imaging of precancer and cancer states of human mucosa. Opt. Express 1997;1:432–440. [PubMed: 19377567]
51. Tearney GJ, Brezinski ME, Bouma BE, Boppart SA, Pitris C, Southern JF, Fujimoto JG. *In vivo* endoscopic optical biopsy with optical coherence tomography. Science 1997;276:2037–2039. [PubMed: 9197265]
52. Boppart SA, Bouma BE, Pitris C, Tearney GJ, Fujimoto JG, Brezinski ME. Forward-imaging instruments for optical coherence tomography. Opt. Lett 1997;22:1618–1620. [PubMed: 18188315]
53. Mak AF, Lai WM, Mow VC. Biphasic indentation of articular-cartilage: 1. Theoretical analysis. J. Biomech 1987;20:703–714. [PubMed: 3654668]
54. Mow VC, Gibbs MC, Lai WM, Zhu WB, Athanasiou KA. Biphasic indentation of articular-cartilage: 2. A numerical algorithm and an experimental study. J. Biomech 1989;22:853–861. [PubMed: 2613721]
55. Yu WP, Blanchard JP. An elastic–plastic indentation model and its solutions. J. Mater. Res 1996;11:2358–2367.
56. Summers, DA. Waterjetting Technology. London: Taylor and Francis; 1995.
57. Suh JK, Spilker RL. Indentation analysis of biphasic articular cartilage—nonlinear phenomena under finite deformation. Trans. ASME, J. Biomech. Eng 1994;116:1–9.
58. Zhang M, Zheng YP, Mak AFT. Estimating the effective Young's modulus of soft tissues from indentation tests—nonlinear finite element analysis of effects of friction and large deformation. Med. Eng. Phys 1997;19:512–517. [PubMed: 9394898]
59. Tonuk E, Silver-Thorn MB. Nonlinear elastic material property estimation of lower extremity residual limb tissues. IEEE Trans. Neural Syst. Rehab. Eng 2003;11:43–53.
60. Lu MH, Zheng YP. Indentation test of soft tissues with curved substrates: a finite element study. Med. Biol. Eng. Comput 2004;42:535–540. [PubMed: 15320464]
61. Kirkpatrick SJ, Wang RK, Duncan DD. OCT-based elastography for large and small deformations. Opt. Express 2006;14:11585–11597. [PubMed: 19529578]
62. Wang RKK, Ma ZH, Kirkpatrick SJ. Tissue Doppler optical coherence elastography for real time strain rate and strain mapping of soft tissue. Appl. Phys. Lett 2006;89:144103.

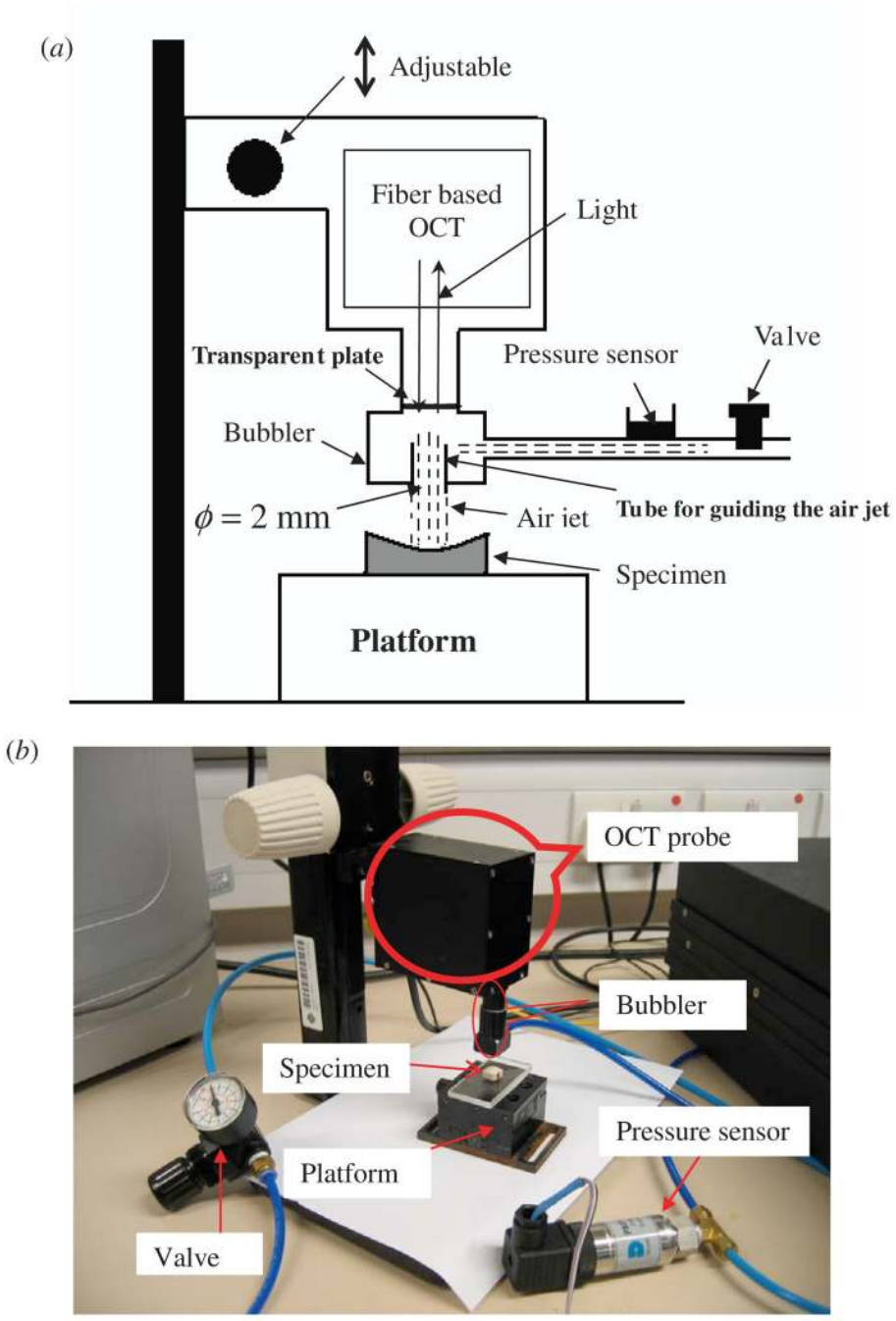

Figure 1.
(*a*) Schematic of the OCT-based air jet indentation system; (*b*) a picture of the real system.

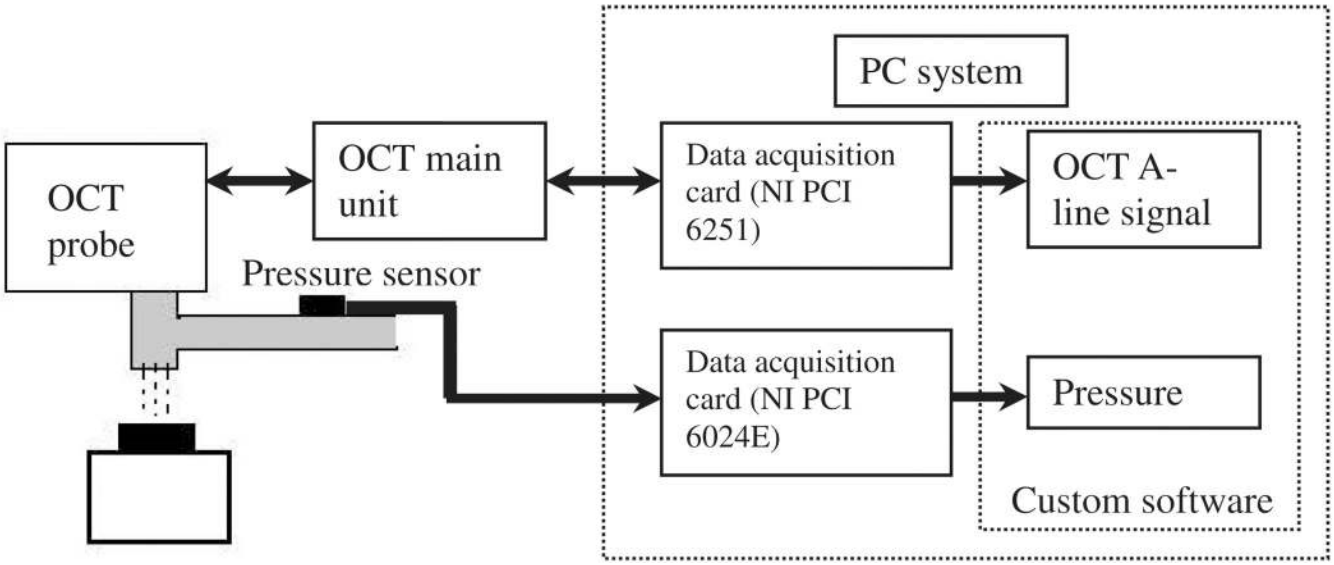

Figure 2.
The diagram of the air jet indentation and data collection modules of the air jet indentation system.

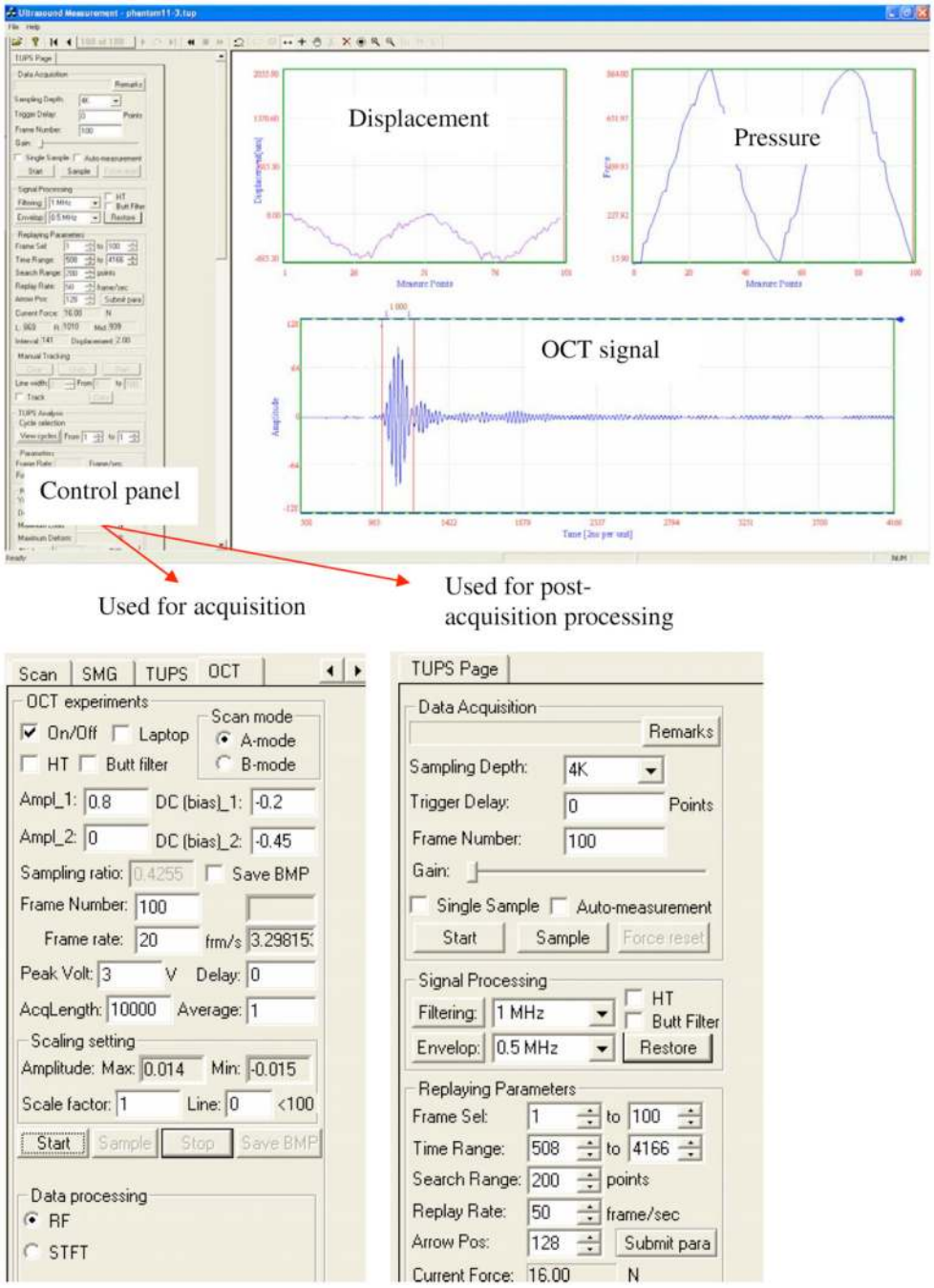

Figure 3.

The custom-designed software interface for the real-time data acquisition and post-acquisition off-line processing such as the displacement extraction. The left of the window shows the control panels for data acquisition and post-acquisition processing. The measured pressure and extracted deformation as well as the OCT signal are displayed on the right.

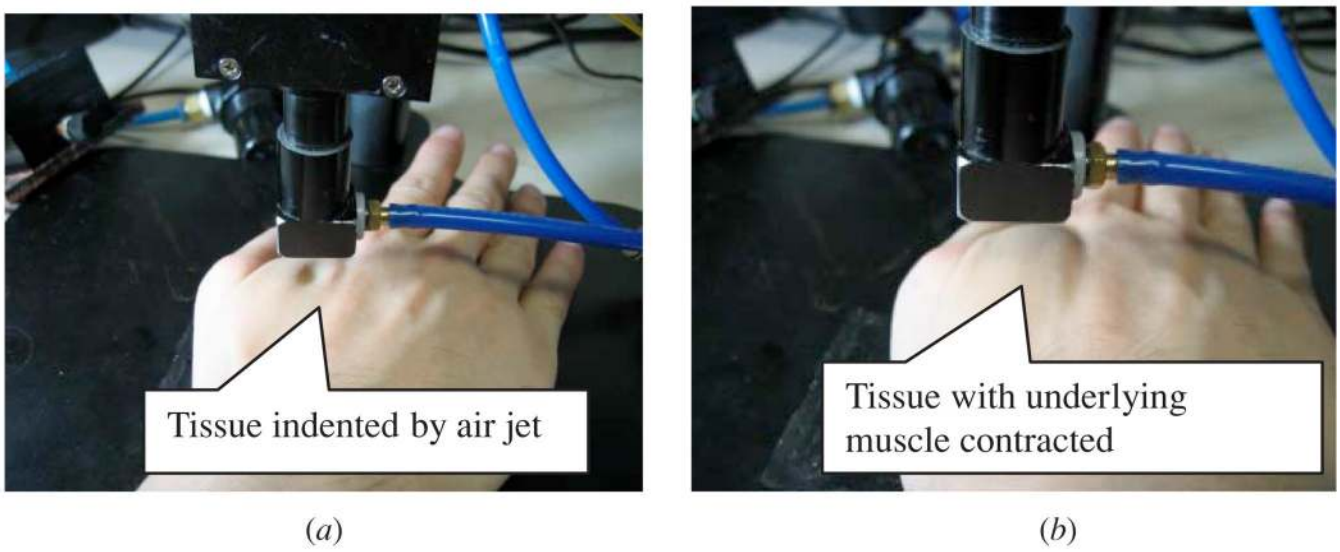

Figure 4.
In vivo experiment on the hand soft tissues: (*a*) soft tissues indented without muscle contraction; (*b*) soft tissues with muscle contraction.

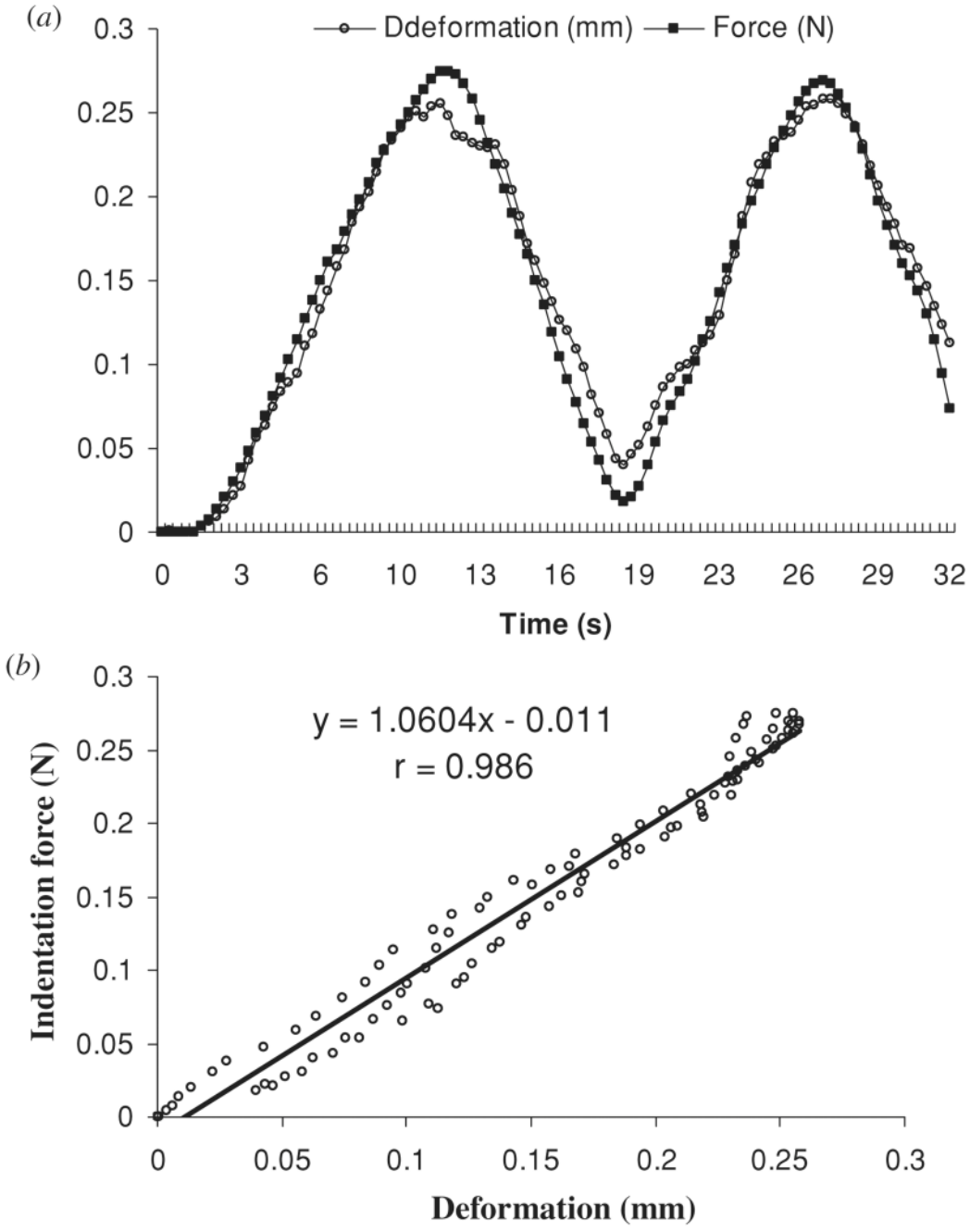

Figure 5.
Representative indentation curves on one phantom: (*a*) force and deformation curves obtained during loading and unloading cycles; (*b*) the relationship between the force and deformation of the phantom.

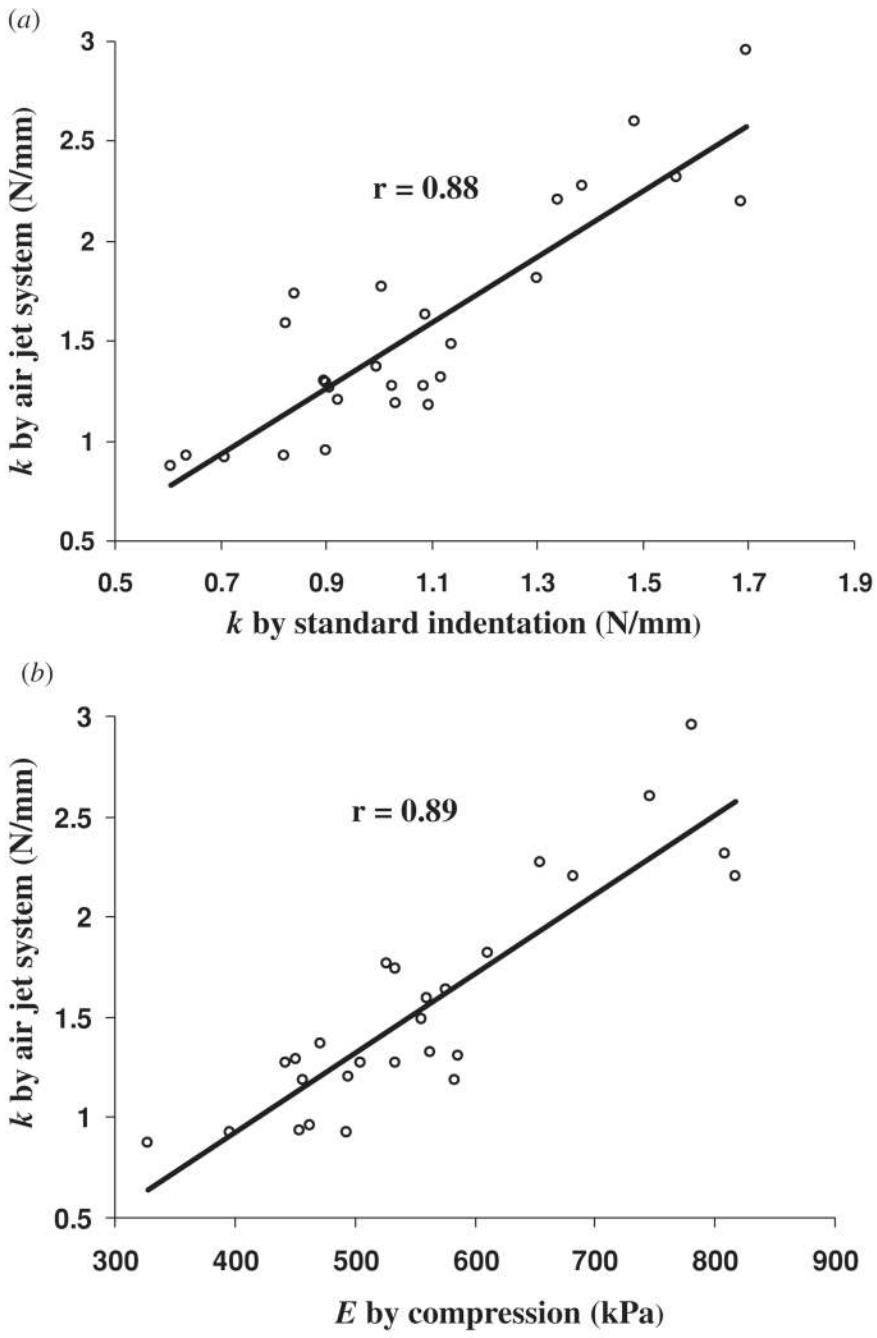

Figure 6.

(*a*) Correlation of stiffness coefficients measured by the air jet and standard indentation tests; (*b*) correlation of stiffness coefficient measured by the air jet indentation test and Young's modulus measured by the standard compression test.